JCAMECH

Vol. 50, No. 1, June 2019, pp 76-89
DOI: 10.22059/jcamech.2019.278583.375

Dynamics, stability analysis and control of a mammal-like octopod robot driven by different central pattern generators

Dariusz Grzelczyk * *and Jan Awrejcewicz*

Department of Automation, Biomechanics and Mechatronics, Lodz University of Technology, 1/15 Stefanowski Street, Lodz, Poland

ARTICLE INFO

Article history:
Received: 31 March 2019
Accepted: 11 April 2019

Keywords:
Octopod
Robot Gait
Legged Motion
Robot Stability
Robot Control

ABSTRACT

In this paper, we studied numerically both kinematic and dynamic models of a biologically inspired mammal-like octopod robot walking with a tetrapod gait. Three different nonlinear oscillators were used to drive the robot's legs working as central pattern generators. In addition, also a new, relatively simple and efficient model was proposed and investigated. The introduced model of the gait generator allowed us to obtain better both kinematic and dynamic parameters of motion of the robot walking in different directions. By changing the length and the height of a single step of the robot, we introduced in a simple way the initial, rhythmic and terminal phases of the robot gait. For numerical research and to visualization of the walking process, we developed a simulation model of the investigated robot in Mathematica software. We computed displacement, velocity and acceleration of the center of the robot's body, fluctuations in the zero moment point of the robot and the ground reaction forces acting on the feet of the robot. The obtained results indicated some advantages of the proposed central pattern generator regarding fluctuations in the robot's body, the minimum value of dynamic stability margin as well as the minimum value of a friction coefficient which is necessary to avoid slipping between the ground and the robot's feet during walking process. Eventually, the proposed model of gait also allowed us to control the vertical position of the robot during walking in different directions.

1. Introduction

Recently, multi-legged robots have gained great popularity in engineering applications and have been widely investigated in the literature. When the legs of the robot are controlled with a degree of autonomy, the robot is able to move and reproduce planned tasks [1]. This is why the legged vehicles inspired by the physiology and anatomy of various animals are a significant group of robots used in different branches of mechanical engineering. Most recently, attention paid to the field of robotics, especially to legged machines that can imitate human or animal movements and substitute people in different tasks, has considerably risen [2].

Interesting literature reviews regarding crab-like robots are presented in some recent papers [2,3]. Aside from numerous crab-like robots, also robots with leg structure modeled on the basis on the anatomy of mammals can also be distinguished (for instance, see papers [1,4,5]). More legs than in quadruped or hexapod robots make the octopods able to overcome more complex obstacles without losing stability. Namely, to form a support polygon and maintain stability of a walking robot, at least three legs are needed, whereas four legs are required to perform the locomotion. As a result, the octopod can still continue its motion even if four of its legs are damaged [5].

Legged robots are challenging in terms of control of their locomotion. However, they can be used in terrains, where wheeled or crawled machines cannot perform their tasks. Namely, legged robots can overcome obstacles of heights equal to the height of their limbs, whereas wheeled robots can overcome obstacles of heights up to the half of the wheel radius [5]. In legged robots, the contact between the ground and the robot's feet takes a form of contact points, on the contrary to wheeled robots, where the contact between the wheels and the ground usually has a continuous character [6]. On the other hand, a large amplitude of the ground reaction force acting on the feet of the robot has a negative influence on the dynamics of the robot, and these forces should be minimized if it is possible. In general, numerous computer programs are used to prototype walking robots before the final construction is created, for instance, see paper [7]. Next, different control strategies of walking robots, as well as their dynamical parameters, are usually tested by different commercial software such as Matlab [1,8],

* Corresponding author. Tel.: +48426312225; fax: +48426312489 ; e-mail: dariusz.grzelczyk@p.lodz.pl

Adams [8,9] or Open Dynamic Engine [10,11], to protect both individual components and the entire mechanism of the robot.

Literature review indicates that studies on walking machines are still challenging and focus attention of numerous researchers. Walking robots with a mammal-like structure of the limbs are characterized by lower stability in comparison to robots with a crab-like structure of legs. In addition, expensive commercial computer software is commonly used to study the dynamics of these vehicles. In this paper, we used Mathematica software to develop kinematical and dynamical models of a mammal-like octopod robot, which are also suitable for estimating crucial parameters of the robot during walking. We studied four central pattern generators (CPGs) controlling the robot's legs, including stability analysis of the robot by using the concept of the zero moment point. Also, we implemented an algorithm suitable for a smooth transition between different gait phased of the robot, i.e., initial, rhythmic and terminal phases [5]. Following much previous research, the employed CPGs have been tested for the robot walking on a planar surface [5,6,12]. Eventually, we also considered the problem of controlling the direction of the robot movement and its vertical position during walking, which is suitable for both the navigation and obstacle avoidance matters in the natural environment. More information in this area can be found in one of the recent papers [2].

The article is organized as follows. Section 2 presents the kinematic/dynamic models and dynamical stability concept for the analysis of the considered mammal-like octopod robot. Section 3 consists of a short literature review devoted to the chosen methods employed to control walking robots and the definitions of the tested CPGs. Section 4 illustrates two (the slowest and the fastest) gaits of eight-legged robots and presents the architecture of the control system used to control the studied robot walking with the tetrapod gait. Some interesting numerical simulations of kinematics, stability, dynamics and control of the analyzed robot are reported and discussed in Section 5. Conclusions from the study are outlined in the last Section 6.

2. Kinematic and dynamic models of an octopod robot

Figure 1 presents a scheme of the studied octopod robot embedded in a global Cartesian coordinate system *Oxyz*, which is fixed to the ground. In addition, a local coordinate system *Cx'y'z'* is fixed to the robot's body (trunk) as it is shown in Fig. 1. The robot has eight identical legs, i.e., four legs on the left side of the trunk (denoted by L1, L2, L3 and L4), and four legs on the right side of the trunk (denoted by R1, R2, R3 and R4). The distances between the legs are equal L in the x' - direction, and H in the y' - direction.

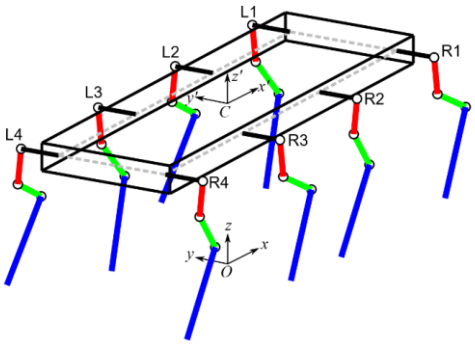

Fig. 1 A scheme of an octopod robot with mammal-like legs.

A schematic configuration of a single mammal-like leg (for instance, leg L4) with three active degrees of freedom (DOFs) is presented in Fig. 2. The mechanism of the robot's leg can be analyzed as a multibody system with three DOFs [5,6]. The leg is located in Earth's gravity field with the standard gravity g = 9.81 m/s^2, and the center of the local coordinate system $O''x''y''z''$ is fixed to the robot's body (see Fig. 2). Coordinates of the centers of local coordinate systems $O''x''y''z''$ for all robot's legs L1, L2, L3, L4, R1, R2, R3 and R4 in the local coordinate system $Cx'y'z'$ fixed to the robot body are as follows: $O''_{L1}(1.5L, 0.5H, 0)$, $O''_{L2}(0.5L, 0.5H, 0)$, $O''_{L3}(-0.5L, 0.5H, 0)$, $O''_{L4}(-1.5L, 0.5H, 0)$, $O''_{R1}(1.5L, -0.5H, 0)$, $O''_{R2}(0.5L, -0.5H, 0)$, $O''_{R3}(-0.5L, -0.5H, 0)$ and $O''_{R4}(-1.5L, -0.5H, 0)$. The parameters m_i and l_i (i = 1,2,3) denote masses and lengths of the links, respectively. The parameters a_i denote the distances between the coordinates of joints and mass centers of the respective links. Angular positions in the joints of the leg are described by the angles $\varphi_i(t)$. $R_x(t)$, $R_y(t)$ and $R_z(t)$ are the components of the ground reaction force acting on the robot's leg in x-, y- and z- directions, respectively. The mass of the trunk (without limbs) is M. Moreover, we assumed that the robot is able to transport an additional load with mass M_L, which is uniformly distributed on the trunk. The values of all parameters required in the numerical simulations were taken from reference [5] and have been depicted in Tab. 1.

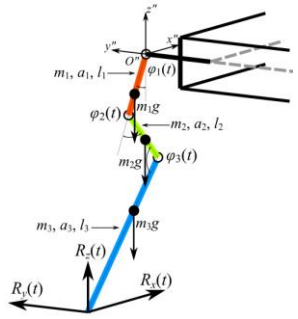

Fig. 2 A schematic drawing of a single mammal-like robot's leg.

Tab. 1 Values of the parameters of the considered octopod robot.

Parameters	Symbol	Unit	Value
Mass of the trunk (without legs)	M	[kg]	1.0
Masses of legs' links (with servos)	m_1; m_2; m_3	[kg]	0.111; 0.140; 0.124
Lengths of legs' links	l_1; l_2; l_3	[m]	0.065; 0.100; 0.165
Positions of links' mass centers	a_1; a_2; a_3	[m]	0.052; 0.075; 0.075
Distances between the legs	L; H	[m]	0.263; 0.210

Forward kinematics for the "foot" of the leg presented in Fig. 2 has the form

$$\begin{cases} x''(t) = l_2 \sin\varphi_2(t) - l_3 \sin\left(\pi - \varphi_2(t) - \varphi_3(t)\right), \\ y''(t) = \left(-l_1 - l_2 \cos\varphi_2(t) - l_3 \cos\left(\pi - \varphi_2(t) - \varphi_3(t)\right)\right)\sin\varphi_1(t), \\ z''(t) = \left(-l_1 - l_2 \cos\varphi_2(t) - l_3 \cos\left(\pi - \varphi_2(t) - \varphi_3(t)\right)\right)\cos\varphi_1(t), \end{cases} \quad (1)$$

whereas the inverse kinematics is given as follows

$$\begin{cases} \varphi_1(t) = \operatorname{atan}\left(\dfrac{y''(t)}{-z''(t)}\right), \\ \varphi_2(t) = \operatorname{atan}\left(\dfrac{x''(t)}{d_1(t)}\right) + \operatorname{acos}\left(\dfrac{l_2^2 + [d_2(t)]^2 - l_3^2}{2l_2 d_2(t)}\right), \\ \varphi_3(t) = \operatorname{acos}\left(\dfrac{l_2^2 + l_3^2 - [d_2(t)]^2}{2l_2 l_3}\right), \end{cases} \tag{2}$$

where $d_1(t) = \sqrt{[y''(t)]^2 + [z''(t)]^2} - l_1$ and $d_2(t) = \sqrt{[d_1(t)]^2 + [x''(t)]^2}$.

In this paper, we investigated a tetrapod gait as one of the most popular and also fastest gaits of octopod robots [5,13]. On the other hand, it is also the least stable gait, which generates the greatest ground reaction forces during walking. In our opinion, all these features make it worth investigating. In the case of the tetrapod gait, the articulated variables $\varphi_{1a}(t)$, $\varphi_{2a}(t)$ and $\varphi_{3a}(t)$ correspond to one group (group *a*) of the robot's legs (L1, L3, R2 and R4), whereas the angles $\varphi_{1b}(t)$, $\varphi_{2b}(t)$ and $\varphi_{3b}(t)$ correspond to the second group (group *b*) of the robot's legs (R1, R3, L2 and L4). Therefore, the variables describing positions of the feet of the legs from groups *a* and *b* in the local coordinate system $O''x''y''z''$ are different and equal $x''_a(t)$, $y''_a(t)$, $z''_a(t)$, and $x''_b(t)$, $y''_b(t)$, $z''_b(t)$, respectively. A diagram of the control system realizing the investigated tetrapod gait is presented in Section 4.

Coordinates $x_C(t)$, $y_C(t)$ and $z_C(t)$ of the robot's center (center of the trunk), marked by point *C* in Fig. 1, in the global coordinate system *Oxyz*, in *x*-, *y*- and *z*- directions (i.e., forward, lateral and vertical directions, respectively), can be calculated as follows

$$x_C(t) = \int_0^t v_{xC}(\tau)d\tau\ ,\ y_C(t) = \int_0^t v_{yC}(\tau)d\tau\ , \tag{3}$$

$$z_C(t) = \begin{cases} -z''_a(t) & \text{if} \quad |z''_a(t)| \geq |z''_b(t)|, \\ -z''_b(t) & \text{if} \quad |z''_a(t)| < |z''_b(t)|, \end{cases} \tag{4}$$

where

$$v_{xC}(t) = \begin{cases} -\dot{x}''_a(t) & \text{if} \quad |z''_a(t)| \geq |z''_b(t)|, \\ -\dot{x}''_b(t) & \text{if} \quad |z''_a(t)| < |z''_b(t)|, \end{cases} \tag{5}$$

$$v_{yC}(t) = \begin{cases} -\dot{y}''_a(t) & \text{if} \quad |z''_a(t)| \geq |z''_b(t)|, \\ -\dot{y}''_b(t) & \text{if} \quad |z''_a(t)| < |z''_b(t)|. \end{cases} \tag{6}$$

In our study, we computed fluctuations in the center of mass of the robot. In the case of the investigated octopod robot, the coordinates of the vector $\mathbf{r}_{COM}(t) = [x_{COM}(t), y_{COM}(t), z_{COM}(t)]^{\mathrm{T}}$, of the spatial position of the center of mass in the global coordinate system *Oxyz* were calculated from the following formula

$$x_{COM}(t) = \frac{\left(M + M_L\right)x_{\mathrm{C}}(t) + \sum_{j=1}^{4}\sum_{i=1}^{3} m_i x_i^{(\mathrm{Lj})}(t) + \sum_{j=1}^{4}\sum_{i=1}^{3} m_i x_i^{(\mathrm{Rj})}(t)}{M + M_L + 8\sum_{i=1}^{3} m_i}, \tag{7}$$

$$y_{COM}(t) = \frac{\left(M + M_L\right)y_{\mathrm{C}}(t) + \sum_{j=1}^{4}\sum_{i=1}^{3} m_i y_i^{(\mathrm{Lj})}(t) + \sum_{j=1}^{4}\sum_{i=1}^{3} m_i y_i^{(\mathrm{Rj})}(t)}{M + M_L + 8\sum_{i=1}^{3} m_i}, \tag{8}$$

$$z_{COM}(t) = \frac{\left(M + M_L\right)z_{\mathrm{C}}(t) + \sum_{j=1}^{4}\sum_{i=1}^{3} m_i z_i^{(\mathrm{Lj})}(t) + \sum_{j=1}^{4}\sum_{i=1}^{3} m_i z_i^{(\mathrm{Rj})}(t)}{M + M_L + 8\sum_{i=1}^{3} m_i}. \tag{9}$$

To study the dynamics and control of the legged locomotion, the so-called Zero Moment Point (ZMP) concept is more useful [14]. This concept assumes the planar contact area and friction high enough to keep the feet from sliding on the ground. This is why we also introduced these assumptions in our study. It should be noted that during walking of the robot, the values of derivatives of moments of the momentum of each segment of the robot are relatively small [15]. Therefore, the coordinates $x_{ZMP}(t)$ and $y_{ZMP}(t)$ of the zero moment point in the global coordinate system *Oxyz* were calculated from the formula

$$x_{ZMP}(t) = \frac{\Sigma_A(t) - \Sigma_B(t)}{\Sigma_E(t)}\ ,\ y_{ZMP}(t) = \frac{\Sigma_C(t) - \Sigma_D(t)}{\Sigma_E(t)}, \tag{10}$$

where

$$\begin{aligned} \Sigma_A(t) &= \left(M + M_L\right)\left(\ddot{z}_{\mathrm{C}}(t) + g_z\right)x_{\mathrm{C}}(t) + \\ &+ \sum_{j=1}^{4}\sum_{i=1}^{3} m_i\left(\ddot{z}_i^{(\mathrm{Lj})}(t) + g_z\right)x_i^{(\mathrm{Lj})}(t) + \\ &+ \sum_{j=1}^{4}\sum_{i=1}^{3} m_i\left(\ddot{z}_i^{(\mathrm{Rj})}(t) + g_z\right)x_i^{(\mathrm{Rj})}(t), \end{aligned} \tag{11}$$

$$\begin{aligned} \Sigma_B(t) &= \left(M + M_L\right)\left(\ddot{x}_{\mathrm{C}}(t) + g_x\right)z_{\mathrm{C}}(t) + \\ &+ \sum_{j=1}^{4}\sum_{i=1}^{3} m_i\left(\ddot{x}_i^{(\mathrm{Lj})}(t) + g_x\right)z_i^{(\mathrm{Lj})}(t) + \\ &+ \sum_{j=1}^{4}\sum_{i=1}^{3} m_i\left(\ddot{x}_i^{(\mathrm{Rj})}(t) + g_x\right)z_i^{(\mathrm{Rj})}(t), \end{aligned} \tag{12}$$

$$\begin{aligned} \Sigma_C(t) &= \left(M + M_L\right)\left(\ddot{z}_{\mathrm{C}}(t) + g_z\right)y_{\mathrm{C}}(t) + \\ &+ \sum_{j=1}^{4}\sum_{i=1}^{3} m_i\left(\ddot{z}_i^{(\mathrm{Lj})}(t) + g_z\right)y_i^{(\mathrm{Lj})}(t) + \\ &+ \sum_{j=1}^{4}\sum_{i=1}^{3} m_i\left(\ddot{z}_i^{(\mathrm{Rj})}(t) + g_z\right)y_i^{(\mathrm{Rj})}(t), \end{aligned} \tag{13}$$

$$\begin{aligned} \Sigma_D(t) &= \left(M + M_L\right)\left(\ddot{y}_{\mathrm{C}}(t) + g_y\right)z_{\mathrm{C}}(t) + \\ &+ \sum_{j=1}^{4}\sum_{i=1}^{3} m_i\left(\ddot{y}_i^{(\mathrm{Lj})}(t) + g_y\right)z_i^{(\mathrm{Lj})}(t) + \\ &+ \sum_{j=1}^{4}\sum_{i=1}^{3} m_i\left(\ddot{y}_i^{(\mathrm{Rj})}(t) + g_y\right)z_i^{(\mathrm{Rj})}(t), \end{aligned} \tag{14}$$

$$\Sigma_E(t) = \left(M + M_L\right)\left(\ddot{z}_C(t) + g_z\right) + \\ + \sum_{j=1}^{4}\sum_{i=1}^{3} m_i\left(\ddot{z}_i^{(\mathrm{L}j)}(t) + g_z\right) + \sum_{j=1}^{4}\sum_{i=1}^{3} m_i\left(\ddot{z}_i^{(\mathrm{R}j)}(t) + g_z\right). \tag{15}$$

Due to the considered planar walking surface and Earth's gravity field, $g_x = 0$, $g_y = 0$ and $g_z = g$.

All components of ground reaction forces acting on the robot's legs were estimated with the use of an inverse dynamics concept, based on the following vector equation written in the global coordinate system *Oxyz*

$$\left(M + M_L\right)\ddot{\mathbf{r}}_C(t) + \sum_{j=1}^{4}\sum_{i=1}^{3} m_i\ddot{\mathbf{r}}_i^{(\mathrm{L}j)}(t) + \sum_{j=1}^{4}\sum_{i=1}^{3} m_i\ddot{\mathbf{r}}_i^{(\mathrm{R}j)}(t) = \\ = \sum_{j=1}^{4}\mathbf{R}^{(\mathrm{L}j)}(t) + \sum_{j=1}^{4}\mathbf{R}^{(\mathrm{R}j)}(t) + \left(M + M_L + 8\sum_{i=1}^{3} m_i\right)\mathbf{g}, \tag{16}$$

where $\mathbf{r}_C(t) = [x_C(t), y_C(t), z_C(t)]^{\mathrm{T}}$ denotes the vector of the center (point *C*) of the trunk of the robot, $\mathbf{r}_i^{(\mathrm{L}j)}(t) = [x_i^{(\mathrm{L}j)}(t), y_i^{(\mathrm{L}j)}(t), z_i^{(\mathrm{L}j)}(t)]^{\mathrm{T}}$ and $\mathbf{r}_i^{(\mathrm{R}j)}(t) = [x_i^{(\mathrm{R}j)}(t), y_i^{(\mathrm{R}j)}(t), z_i^{(\mathrm{R}j)}(t)]^{\mathrm{T}}$ are vectors of the positions of the mass centers of individual links of the robot's legs on the left and right side of the trunk, respectively, $\mathbf{R}^{(\mathrm{L}j)}(t) = [R_x^{(\mathrm{L}j)}(t), R_y^{(\mathrm{L}j)}(t), R_z^{(\mathrm{L}j)}(t)]^{\mathrm{T}}$ and $\mathbf{R}^{(\mathrm{R}j)}(t) = [R_x^{(\mathrm{R}j)}(t), R_y^{(\mathrm{R}j)}(t), R_z^{(\mathrm{R}j)}(t)]^{\mathrm{T}}$ denote ground reaction forces acting on the feet during the interaction with the ground, whereas $\mathbf{g} = [0, 0, -g]^{\mathrm{T}}$ is the vector of Earth's gravity. The above-presented vector equation can be rewritten in the following scalar forms

$$\left(M + M_L\right)\ddot{x}_C(t) + \sum_{j=1}^{4}\sum_{i=1}^{3} m_i\ddot{x}_i^{(\mathrm{L}j)}(t) + \sum_{j=1}^{4}\sum_{i=1}^{3} m_i\ddot{x}_i^{(\mathrm{R}j)}(t) = \\ = \sum_{j=1}^{4} R_x^{(\mathrm{L}j)}(t) + \sum_{j=1}^{4} R_x^{(\mathrm{R}j)}(t), \tag{17}$$

$$\left(M + M_L\right)\ddot{y}_C(t) + \sum_{j=1}^{4}\sum_{i=1}^{3} m_i\ddot{y}_i^{(\mathrm{L}j)}(t) + \sum_{j=1}^{4}\sum_{i=1}^{3} m_i\ddot{y}_i^{(\mathrm{R}j)}(t) = \\ = \sum_{j=1}^{4} R_y^{(\mathrm{L}j)}(t) + \sum_{j=1}^{4} R_y^{(\mathrm{R}j)}(t), \tag{18}$$

$$\left(M + M_L\right)\ddot{z}_C(t) + \sum_{j=1}^{4}\sum_{i=1}^{3} m_i\ddot{z}_i^{(\mathrm{L}j)}(t) + \sum_{j=1}^{4}\sum_{i=1}^{3} m_i\ddot{z}_i^{(\mathrm{R}j)}(t) + \\ + \left(M + M_L + 8\sum_{i=1}^{3} m_i\right)g = \sum_{j=1}^{4} R_z^{(\mathrm{L}j)}(t) + \sum_{j=1}^{4} R_z^{(\mathrm{R}j)}(t). \tag{19}$$

The robot's legs are in stance (i.e., in contact with the ground) in one gait phase, whereas they perform swing movements (i.e., there is no contact with the ground) in the other phase. Because of the symmetrical distribution of the robot's legs, the lack of rotation of the robot's trunk during walking, as well as partial mutual compensations of the movements of individuals segments of the robot legs, we can assume that

$$R_x^{(L1)}(t) = R_x^{(L3)}(t) = R_x^{(R2)}(t) = R_x^{(R4)}(t) = R_{ax}(t)\,, \tag{20}$$

$$R_x^{(L2)}(t) = R_x^{(L4)}(t) = R_x^{(R1)}(t) = R_x^{(R3)}(t) = R_{bx}(t)\,, \tag{21}$$

$$R_y^{(L1)}(t) = R_y^{(L3)}(t) = R_y^{(R2)}(t) = R_y^{(R4)}(t) = R_{ay}(t)\,, \tag{22}$$

$$R_y^{(L2)}(t) = R_y^{(L4)}(t) = R_y^{(R1)}(t) = R_y^{(R3)}(t) = R_{by}(t)\,, \tag{23}$$

$$R_z^{(L1)}(t) = R_z^{(L3)}(t) = R_z^{(R2)}(t) = R_z^{(R4)}(t) = R_{az}(t)\,, \tag{24}$$

$$R_z^{(L2)}(t) = R_z^{(L4)}(t) = R_z^{(R1)}(t) = R_z^{(R3)}(t) = R_{bz}(t)\,. \tag{25}$$

In order to assess the dynamic properties of the investigated CPGs, we introduced functions $\mu_{ax}(t)$, $\mu_{bx}(t)$, $\mu_{ay}(t)$ and $\mu_{by}(t)$, calculated for the legs which are in contact with the ground

$$\mu_{ax}(t) = \frac{R_{ax}(t)}{R_{az}(t)}\,,\ \mu_{bx}(t) = \frac{R_{bx}(t)}{R_{bz}(t)}\,, \tag{26}$$

$$\mu_{ay}(t) = \frac{R_{ay}(t)}{R_{az}(t)}\,,\ \mu_{by}(t) = \frac{R_{by}(t)}{R_{bz}(t)}\,. \tag{27}$$

The detailed analysis of these functions allowed us to estimate the minimum value of the friction coefficient in each phase of the robot gait, which is necessary to avoid slipping between the ground and the robot's feet. When the robot moves in an arbitrary direction, all components $R_x(t)$, $R_y(t)$ and $R_z(t)$ of ground reaction forces should be considered. Therefore, the minimum value of the coefficient of friction that makes it possible to avoid slipping between the ground and the feet of the robot in each phase of gait (i.e., phase *a* and phase *b*), can be computed from the following formula

$$\mu_a(t) = \frac{\sqrt{R_{ax}^2(t) + R_{ay}^2(t)}}{R_{az}(t)}\,,\ \mu_b(t) = \frac{\sqrt{R_{bx}^2(t) + R_{by}^2(t)}}{R_{bz}(t)}\,. \tag{28}$$

3. Central pattern generators

In order to control angular positions in the joints of individual robot's legs, we employed a method based on the inverse kinematic relations with periodic functions forming a network. This approach resembles the operation of neural networks that generate rhythmic outputs in the absence of rhythmic input [16,17]. Such networks have been found by biologists in different biological periodic processes, including swimming, running, breathing, flying, chewing or walking. These processes are controlled by a part of a spinal cord for the vertebrate or by the ganglion for the invertebrate, known as the Central Pattern Generator (CPG) [18,19], which is the source of tightly-coupled patterns of neural activity that does not require sensory information [5,17]. For four last decades, this concept has been commonly applied to control different kinds of bio-inspired walking robots. Also recently, some researchers have employed this approach to control the robot's legs. In general, CPGs as locomotion controllers have been developed with digital processors or analog circuits (see, for instance, papers [13,17]). In our study, we selected and employed three popular nonlinear oscillators working as CPG models, i.e. Hopf oscillator [9,20], hybrid van der Pol-Rayleigh oscillator [21] and Toda-Rayleigh lattice [22-24]. Then, we proposed a novel model of CPG that can be used to control the robot locomotion, and next, we compared it with the above-mentioned nonlinear oscillators.

Two uncoupled Hopf oscillators are governed by the following first-order ordinary differential equations (ODEs)

$$\begin{cases} \dot{u}_a(t) = \left(\sigma - u_a^2(t) - v_a^2(t)\right)u_a(t) + \omega v_a(t), \\ \dot{v}_a(t) = \left(\sigma - u_a^2(t) - v_a^2(t)\right)v_a(t) - \omega u_a(t), \\ \dot{u}_b(t) = \left(\sigma - u_b^2(t) - v_b^2(t)\right)u_b(t) + \omega v_b(t), \\ \dot{v}_b(t) = \left(\sigma - u_b^2(t) - v_b^2(t)\right)v_b(t) - \omega u_b(t), \end{cases} \tag{29}$$

and are further referred to as CPG1. Two uncoupled hybrid van der Pol-Rayleigh oscillators are described by the first-order ODEs

$$\begin{cases} \dot{u}_a(t) = v_a(t), \\ \dot{v}_a(t) = \varepsilon\left(1 - u_a^2(t)\right)v_a(t) + \delta\left(1 - v_a^2(t)\right)v_a(t) - \omega^2 u_a(t), \\ \dot{u}_b(t) = v_b(t), \\ \dot{v}_b(t) = \varepsilon\left(1 - u_b^2(t)\right)v_b(t) + \delta\left(1 - v_b^2(t)\right)v_b(t) - \omega^2 u_b(t), \end{cases} \tag{30}$$

and are further referred to as CPG2. The Toda-Rayleigh lattice is governed by the first-order ODEs

$$\begin{cases} \dot{u}_a(t) = v_a(t), \\ \dot{v}_a(t) = \omega^2\left(e^{u_b(t)-u_a(t)} - e^{u_a(t)-u_b(t)}\right) + \eta\left(1 - v_a^2(t)\right)v_a(t), \\ \dot{u}_b(t) = v_b(t), \\ \dot{v}_b(t) = \omega^2\left(e^{u_a(t)-u_b(t)} - e^{u_b(t)-u_a(t)}\right) + \eta\left(1 - v_b^2(t)\right)v_b(t), \end{cases} \tag{31}$$

and is further referred to as CPG3. In turn, the proposed CPG model (further referred to as CPG4) is governed by the following periodic functions

$$\begin{cases} u_a(t) = f_x\left(\mathrm{mod}[t,T]\right), \\ v_a(t) = f_{za}\left(\mathrm{mod}[t,T]\right), \\ u_b(t) = -u_1(t), \\ v_b(t) = f_{zb}\left(\mathrm{mod}[t,T]\right), \end{cases} \tag{32}$$

where

$$f_x(t) = \begin{cases} \dfrac{2}{T}t & \text{if} \quad t \in [0,\ 0.25T], \\ \dfrac{1}{2} - \dfrac{2}{T}(t - 0.25T) & \text{if} \quad t \in (0.25T,\ 0.75T], \\ -\dfrac{1}{2} + \dfrac{2}{T}(t - 0.75T) & \text{if} \quad (0.75T,\ T], \end{cases} \tag{33}$$

$$f_{za}(t) = \begin{cases} \sin^2\left(\dfrac{2\pi}{T}(t + 0.25T)\right) & \text{if} \quad t \in [0,\ 0.25T], \\ 0 & \text{if} \quad t \in (0.25T,\ 0.75T], \\ -\sin\left(\dfrac{2\pi}{T}(t + 0.75T)\right) & \text{if} \quad (0.75T,\ T], \end{cases} \tag{34}$$

$$f_{zb}(t) = f_{za}(\mathrm{mod}[t - 0.5T, T]), \tag{35}$$

are the functions defined in the time range $t \in [0,\ T]$ (T is the period of a single robot stride). The proposed model of CPG is relatively simple in comparison to other nonlinear oscillators working as CPGs. On the contrary to classical nonlinear oscillators working as CPGs, the proposed model does not require solving nonlinear differential equations, which is advantageous when it comes to implementing control algorithms in a form of a program written for a microcontroller with limited computing power.

In the above CPGs, $u_a(t)$, $v_a(t)$, $u_b(t)$ and $v_b(t)$ denote dimensionless variables, whereas σ, ε, δ, η and ω are constant dimensionless parameters. Examples of stable periodic orbits of the considered CPGs are reported in Fig. 3. The values of abovementioned parameters (σ = 6, ε = 4, δ = 0.4, η = 6 and ω = *2*) were based on the literature and were set so as to obtain significant differences between the trajectories plotted by the robot's feet.

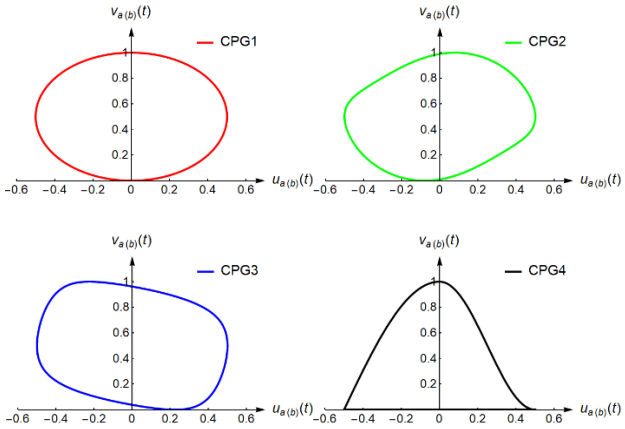

Fig. 3 Normalized stable periodic orbits used as CPGs (σ = 6, ε = 4, δ = 0.4, η = 6 and ω = *2*).

One can find numerous papers focused on implementing the Hopf oscillator [25-28], the van der Pol oscillator [21,29-32], the Rayleigh oscillator [21,29,30], the Toda-Rayleigh lattice [6,13,33], and many others, to generate rhythmic movements of the bio-inspired machines. The CPG model proposed in this paper has some advantages in comparison to the above-mentioned examples, which is illustrated and discussed in further sections of this paper.

4. Architecture of the control system of a robot walking with a tetrapod gait

Since control of mobile robots is a complex engineering problem that requires high coordination of all robot's legs, the control system must select one of numerous alternative movements, depending on the actual situation and/or energetic cost [34]. For instance, a good example of naturally occurring transitions of rhythmic movements can be observed in a horse which can use various gaits, including walk, trot and gallop [17].

Different kinds of gait can be presented schematically by so-called gait timing diagrams [9]. In addition, a duty factor β is usually defined, which denotes the fraction of the cycle time that each foot spends touching the ground (i.e., in the stance). To illustrate it schematically, we presented two typical gaits of the eight-legged robots, i.e., the slowest wave gait (β = 7/8) and the fastest tetrapod gait (β = 1/2) in Fig. 4.

(a) wave gait

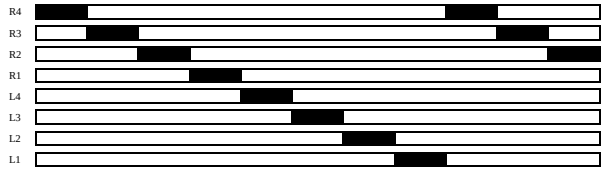

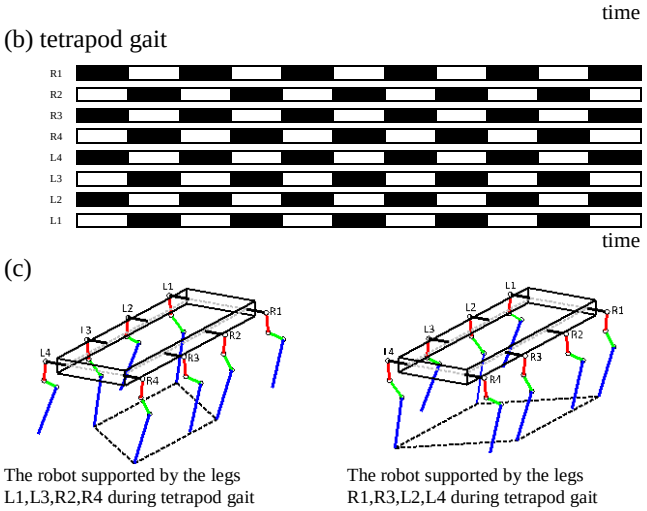

Fig. 4 Diagrams showing the slowest wave gait (a) and the fastest tetrapod gait (b) of an octopod, as well as configurations of the robot's legs in two different phases of the tetrapod gait (c). On the presented diagrams, white color denotes the stance, whereas black color denotes the swing of the robot's legs.

Figure 5 shows schematically a method to generate articulated variables for the joints of each robot's leg.

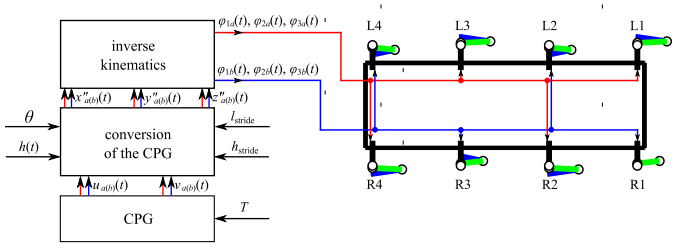

Fig. 5 Algorithm presenting the generation of values of angular positions for each joint driving the legs of the investigated robot.

The normalized periodic orbits of the CPG with the regulated time period T are converted into the workspace of the robot leg, taking into account the parameters l_{stride}, h_{stride}, θ, and function $h(t)$. The parameters l_{stride} and h_{stride} are responsible for the length and the height of a single robot stride, the angle θ controls the direction of movement of the robot with respect to the global coordinate system $Oxyz$ fixed to the ground, while the function $h(t)$ controls the vertical position of the robot. Variables $x''_a(t)$, $x''_b(t)$, $y''_a(t)$, $y''_b(t)$, $z''_a(t)$ and $z''_b(t)$ are obtained by converting the variables $u_a(t)$, $v_a(t)$, $u_b(t)$, $v_b(t)$ of the CPG to the workspace of the leg's mechanism by using the following formula

$$x''_a(t) = l_{\text{stride}} \cdot u_a(t) \cdot \cos\theta\,, \tag{36}$$

$$x''_b(t) = l_{\text{stride}} \cdot u_b(t) \cdot \cos\theta\,, \tag{37}$$

$$y''_a(t) = l_{\text{stride}} \cdot u_a(t) \cdot \sin\theta\,, \tag{38}$$

$$y''_b(t) = l_{\text{stride}} \cdot u_b(t) \cdot \sin\theta\,, \tag{39}$$

$$z''_a(t) = h_{\text{stride}} \cdot v_a(t) - h(t)\,, \tag{40}$$

$$z''_b(t) = h_{\text{stride}} \cdot v_b(t) - h(t)\,. \tag{41}$$

In the next step, the obtained variables are converted into the joint space $\varphi_{1a}(t)$, $\varphi_{2a}(t)$, $\varphi_{3a}(t)$ and $\varphi_{1b}(t)$, $\varphi_{2b}(t)$, $\varphi_{3b}(t)$ by using the inverse kinematics relations (2). The angles $\varphi_{1a}(t)$, $\varphi_{2a}(t)$, $\varphi_{3a}(t)$ control the joints of the legs L1, L3, R2 and R4 (the group a of the robot legs), whereas the angles $\varphi_{1b}(t)$, $\varphi_{2b}(t)$, $\varphi_{3b}(t)$ control the joints of the legs R1, R3, L2 and L4 (the group b of the robot legs). As a result, the robot is supported by the legs from the group a in one phase, and by the legs from group b in the other one (see Fig. 4). Figure 6 illustrates examples of trajectories plotted by a single robot leg in the local coordinate system $O''x''y''z''$, both in x''-z'' and y''-z'' planes. Time histories of the articulated angular positions $\varphi_{1a}(t)$, $\varphi_{2a}(t)$, $\varphi_{3a}(t)$ and $\varphi_{1b}(t)$, $\varphi_{2b}(t)$, $\varphi_{3b}(t)$ are presented in Fig. 7. The articulated variables applied to the legs' joints cause the robot movement in the global coordinate system $Oxyz$, along the direction defined by the angle θ. In our control method, the axes x', y', z' of the local coordinate system $Cx'y'z'$ are parallel to the axes x, y, z of the global coordinate system $Oxyz$ during the whole locomotion process. As a result, we focus on forward, lateral and oblique movements of the robot, while the rotation of the robot's trunk in the coordinate system $Oxyz$ is outside of the area of interest of this study.

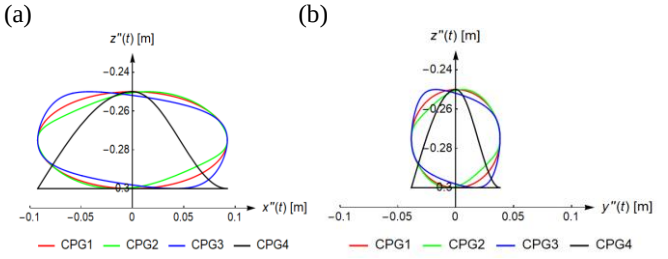

Fig. 6 The periodic orbits of different CPGs converted into the workspace of a single robot leg in the plane x''-z'' (a), and in the plane y''-z'' (b). The trajectories were calculated for the following parameters: T = 2 s, l_{stride} = 0.2 m, h_{stride} = 0.05 m, θ = π/8 and $h(t)$ = 0.3 m.

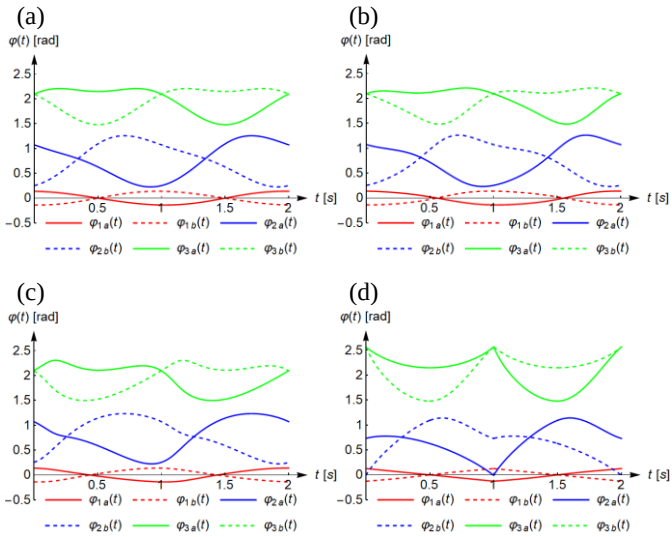

Fig. 7 Time histories of the angles $\varphi_{1a}(t)$, $\varphi_{2a}(t)$, $\varphi_{3a}(t)$ and $\varphi_{1b}(t)$, $\varphi_{2b}(t)$, $\varphi_{3b}(t)$ in a single stride for T = 2 s, l_{stride} = 0.2 m, h_{stride} = 0.05 m, θ = π/8 and $h(t)$ = 0.3 m and different CPGs, i.e. CPG1 (a); CPG2 (b); CPG3 (c) and CPG4 (d).

5. Numerical simulations

Figure 8 shows the developed 3D full parametric simulation model of the investigated octopod robot implemented in Mathematica. The created model allowed us to visualize the robot during walking as well as control the correctness of the simulated results, especially the spatial position of individual elements of the robot and the configurations of the legs. The robot located in the coordinate system *Oxyz* fixed to the ground (green surface) is represented by the trunk (gray cuboid) and eight legs (each leg is composed of three links represented by red, green and blue lines, respectively). We also animated all joints of the legs (yellow cylinders), centers of masses of the legs' links (gray balls) and the supporting polygon (bounded by black dashed lines).

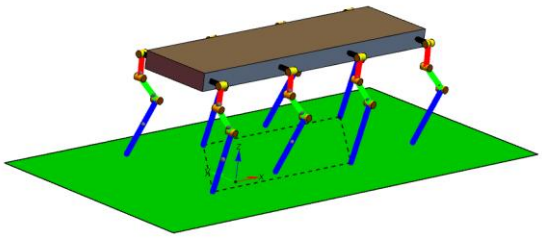

Fig. 8 Simulation model of the investigated octopod robot, created in Mathematica.

Figures 9-11 show time histories of displacements $x_C(t)$, $y_C(t)$, $z_C(t)$, velocities $v_{xC}(t)$, $v_{yC}(t)$, $v_{zC}(t)$ and accelerations $a_{xC}(t)$, $a_{yC}(t)$, $a_{zC}(t)$ of the robot's center (point C in Fig. 1) in the x-, y- and z-directions, respectively. These kinematic quantities were obtained for a single robot stride of the rhythmic tetrapod gait (in time from 0 to T) and for different CPGs. We assumed that the beginning of a stride corresponds to the beginning of the support by the legs L1, L3, R2 and R4, and that it starts from the initial position, i.e., $x_C(t) = 0$ and $y_C(t) = 0$. Due to the changing supporting polygon of the robot, time histories of the crucial kinematic parameters have nonsmooth or discontinuous character. Significant differences between the presented parameters are clearly visible for the three well-known nonlinear oscillators, i.e., CPG1, CPG2 and CPG3. Moreover, fluctuations in the vertical position of the robot are also clearly visible for these CPGs, although $h(t)$ = const. Fluctuations in both the velocities and the accelerations are not observed for the robot's motion driven by the proposed CPG models.

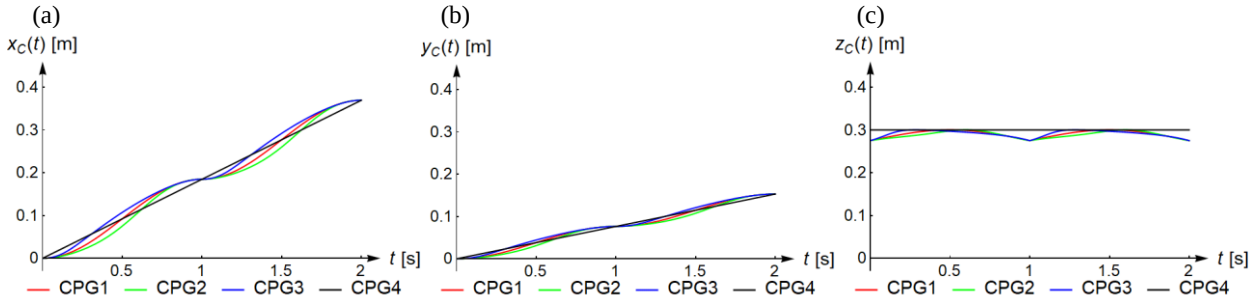

Fig. 9 Fluctuations in displacements $x_C(t)$ (a), $y_C(t)$ (b), and $z_C(t)$ (c) of the robot in the forward, lateral and vertical directions, respectively, obtained for a single stride of the robot driven by different CPGs.

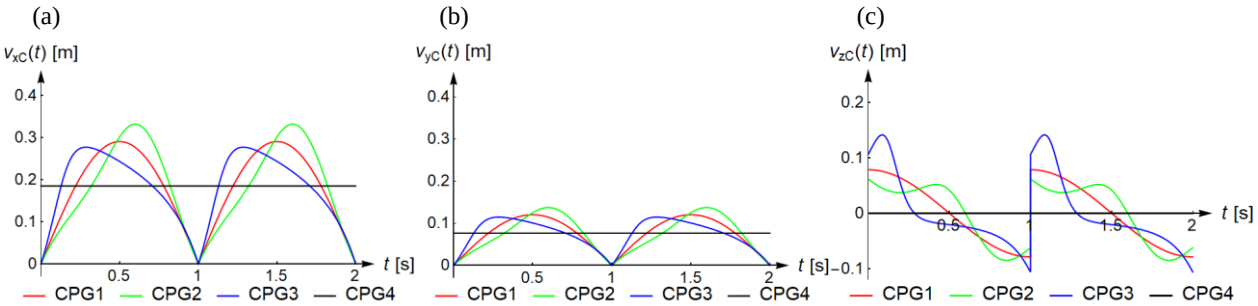

Fig. 10 Fluctuations in velocities $v_{xC}(t)$ (a), $v_{yC}(t)$ (b), and $v_{zC}(t)$ (c) of the robot in the forward, lateral and vertical directions, respectively, obtained for a single stride of the robot driven by different CPGs.

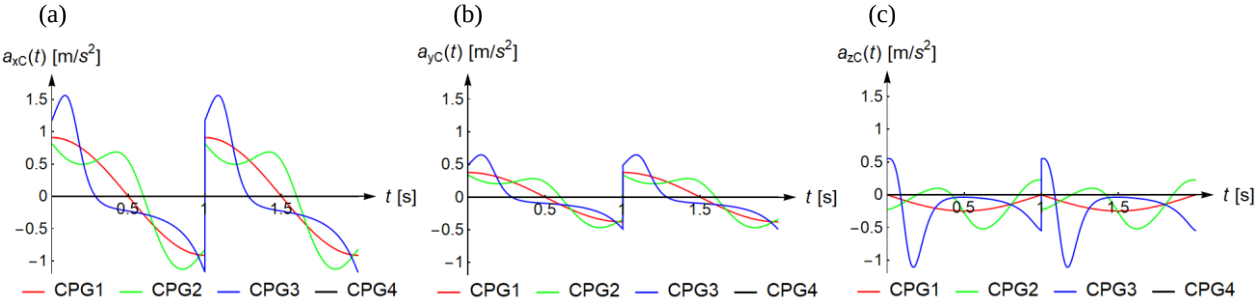

Fig. 11 Fluctuations in accelerations $a_{xC}(t)$ (a), $a_{yC}(t)$ (b), and $a_{zC}(t)$ (c) of the robot in the forward, lateral and vertical directions, respectively, obtained for a single stride of the robot driven by different CPGs.

Figure 12 presents the curves of trajectories of the ZMP, plotted for all four investigated CPGs, as well as supporting polygons of the robot, which are represented by black dashed lines. In these simulations, we used the same values of parameters as before. For all used models of CPGs, the trajectories of the ZMP points lie inside the supporting polygon of the robot. Therefore, the movement of the robot is stable in all presented cases. It should be noted that in the case of CPG4, the fluctuations in the ZMP are the lowest and farthest from the edges of the supporting polygons. Therefore, when the robot is driven by the proposed CPG, its movement is the most stable.

(a)

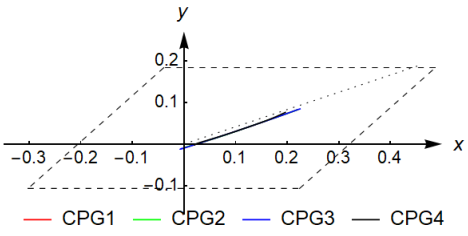

(b)

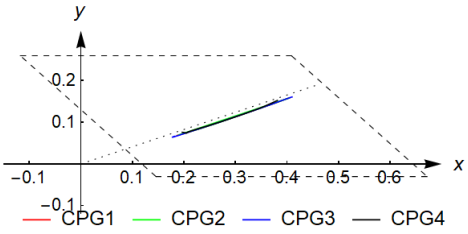

Fig. 12 Fluctuations in the ZMP calculated for the phase *a* (a) and the phase *b* (b) of a single stride of the robot driven by different CPGs.

A more detailed analysis of the dynamical stability of the robot comprises the investigation of the trajectories $x_{ZMP}(t)$-$y_{ZMP}(t)$, plotted in the coordinate system *Oxyz*, including the supporting polygons of the robot. By using the simulation model developed in Mathematica, in Fig. 13, we plotted the position of the ZMP (red dot), the projection of the position of the center of mass (blue dot), the projection of the position of the center of the robot body (black dot), the contour of the robot's trunk (gray rectangle) as well as the supporting polygon (gray dashed lines), on the plane *x*-*y* of the coordinate system *Oxyz*. The supporting legs are represented by the solid (red, green and blue) lines, while the legs in the swing phase are represented by the dashed (red, green and blue) lines, respectively. Moreover, the red line represents the distance between the edge of the supporting polygon and the ZMP, calculated in the direction of the robot's movement. The calculated distance *DSM*(*t*) is the dynamic stability margin (DSM).

(a) phase *a* of a single robot stride

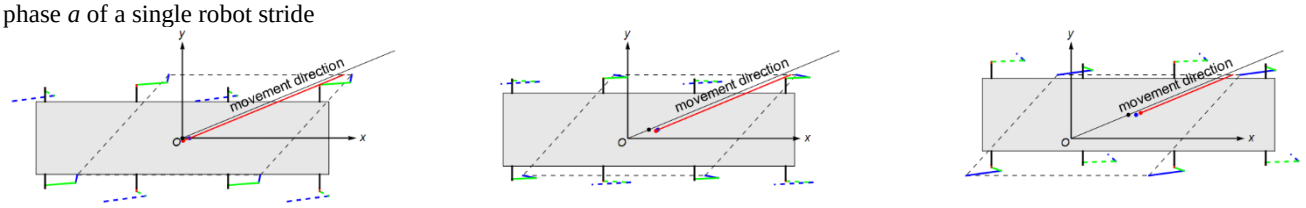

t = 0 s *t* = 0.4 s *t* = 0.8 s

(b) phase *b* of a single robot stride

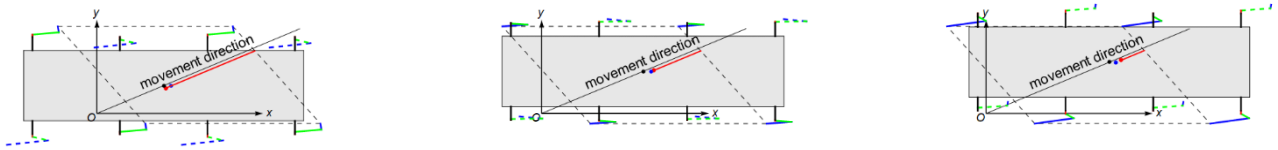

t = 1.2 s *t* = 1.6 s *t* = 2.0 s

Fig. 13 Top view of the walking process of the investigated robot simulated in Mathematica and captured at regular time intervals.

The computed distance representing the dynamical stability margin changes in time, in both phases of a single rhythmic robot stride (see Fig. 14). For all used CPGs, for $t = T/2$, discontinuity of the functions *DSM*(*t*) can be observed, which results from changes in the supporting polygon.

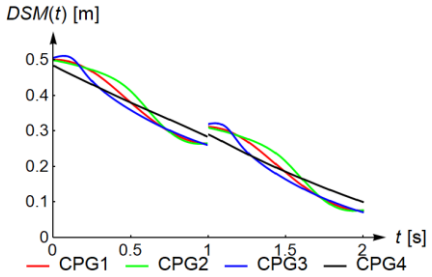

Fig. 14 $DSM(t)$ obtained for a single rhythmic stride of the robot driven by different CPGs.

The stability analysis can be interpreted by different coefficients. In our study, we calculated the minimum value of the function $DSM(t)$ in the range of the time of a single stride, namely

$$DSM_{\min} = \min_{t\in[0,T]} DSM(t), \tag{42}$$

which can be used as a coefficient assessing the dynamical stability of the robot. Figure 15 shows values of the introduced parameter $DSM_{\min}$ obtained for the angles θ in the range $\theta \in [0, 2\pi]$. An analysis of the presented results shows that, regardless of the used CPG, the value of the parameter $DSM_{\min}$ (i.e., dynamical stability margin) changes significantly with the change in the θ parameter. The robot has the largest stability during walking in the forward direction ($\theta = 0$ and $\theta = 2\pi$) and the backward direction ($\theta = \pi$). In turn, it is characterized by the smallest stability during walking in the lateral directions (i.e. $\theta = \pi/2$ and $\theta = 3\pi/2$). However, regardless of the parameter θ, the robot's stability is significantly larger when the robot is driven by the proposed CPG model.

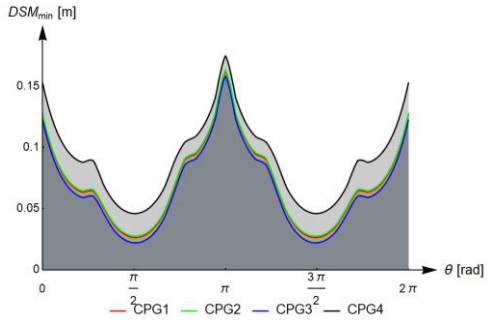

Fig. 15 Values of the $DSM_{\min}$ calculated for different directions of the robot controlled by the parameter θ for different CPGs controlling the robot's legs.

In our study, we also calculated $DSM_{\min}$ for different values of parameters M_L, T, l_{stride} and h_{stride} of a robot walking in different directions θ and driven by different CPGs. Through a detailed analysis of the results presented in Figs. 16-19, it can be stated that the used CPGs, different directions θ of the robot movements and the parameters M_L, T, l_{stride} and h_{stride} have a significant influence on the calculated values of the coefficient $DSM_{\min}$. The benefits of using the proposed CPG model are especially visible for small values of the parameter T, i.e., when the robot is moving at relatively high speed. Moreover, among the three tested cases of the movement direction θ, the robot has the highest stability during walking in the forward direction, i.e., for $\theta = 0$, while the smallest stability was detected for the lateral direction, i.e., $\theta = \pi/2$.

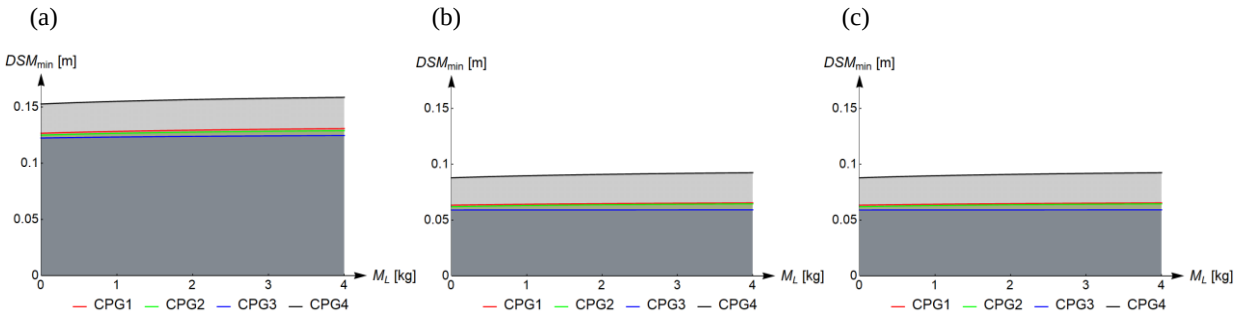

Fig. 16 $DSM_{\min}$ calculated for different values of the parameter M_L, different CPGs and different directions θ of the robot gait: (a) $\theta = 0$; (b) $\theta = \pi/4$; (c) $\theta = \pi/2$.

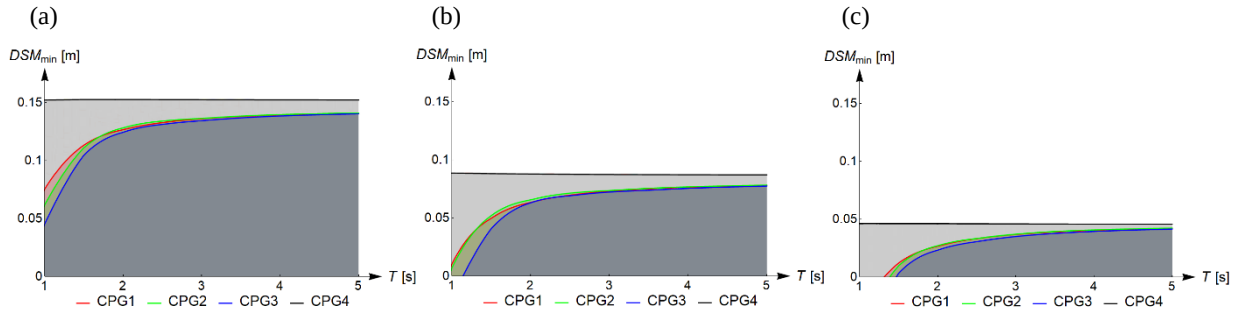

Fig. 17 $DSM_{\min}$ calculated for different values of the parameter T, different CPGs and different directions θ of the robot gait: (a) $\theta = 0$; (b) $\theta = \pi/4$; (c) $\theta = \pi/2$.

(a) (b) (c)

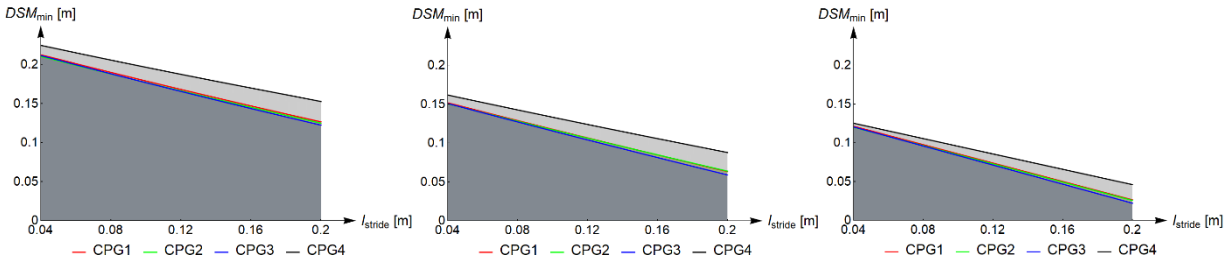

Fig. 18 DSM_{min} calculated for different values of the parameter l_{stride}, different CPGs and different directions θ of the robot gait: (a) θ = 0; (b) $\theta = \pi/4$; (c) $\theta = \pi/2$.

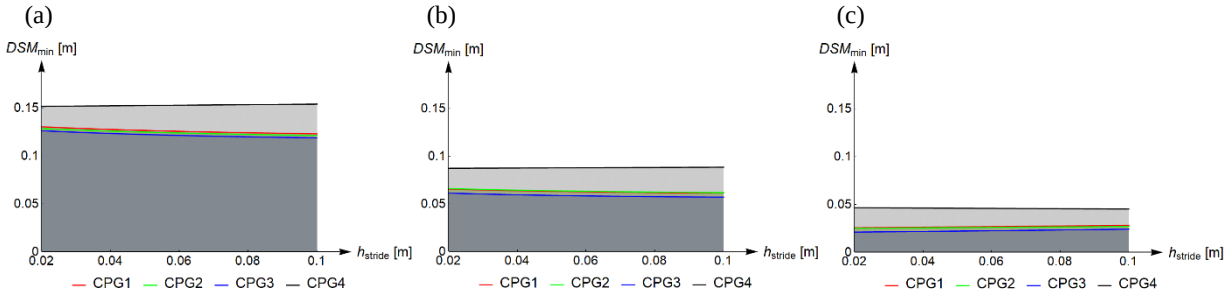

Fig. 19 DSM_{min} calculated for different values of the parameter h_{stride}, different CPGs and different directions θ of the gait: (a) θ = 0; (b) $\theta = \pi/4$; (c) $\theta = \pi/2$.

Figures 20-21 show time histories of the components $R_x(t)$, $R_y(t)$ and $R_z(t)$ of the ground reaction forces (GRFs) acting on the robot's legs, obtained for different CPGs. The results were calculated in Mathematica as a solution to the inverse dynamic problem for the following values of parameters: T = 2 s, l_{stride} = 0.1 m, h_{stride} = 0.05 m, $\theta = \pi/8$ and $h(t)$ = 0.3 m. In all presented cases, fluctuations in all components of the GRFs were detected, but relatively large fluctuations are present for CPG1, CPG2 and CPG3, in comparison to the CPG4. The values of the components $R_z(t)$ fluctuate around the value resulting from the robot weight per one supporting leg, i.e., $R_{gr}(t)$ = 9.81 N.

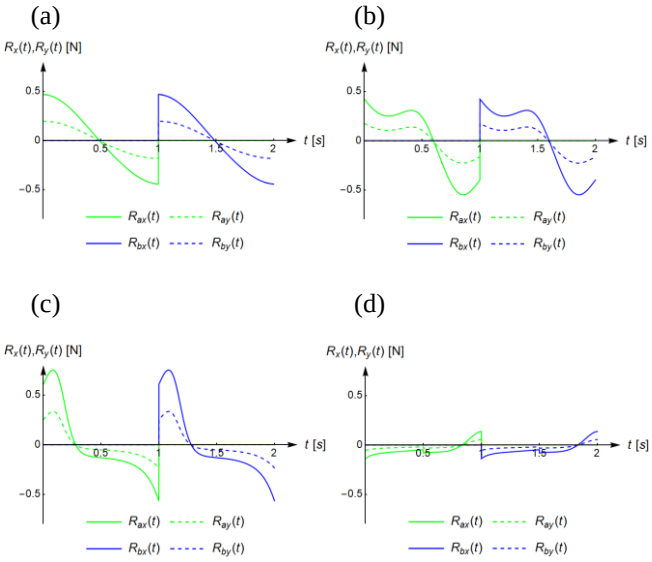

Fig. 20 The components $R_x(t)$ and $R_y(t)$ of the ground reaction force acting of the legs of the robot driven by different CPGs: (a) CPG1; (b) CPG2; (c) CPG3; (d) CPG4.

(a) (b)

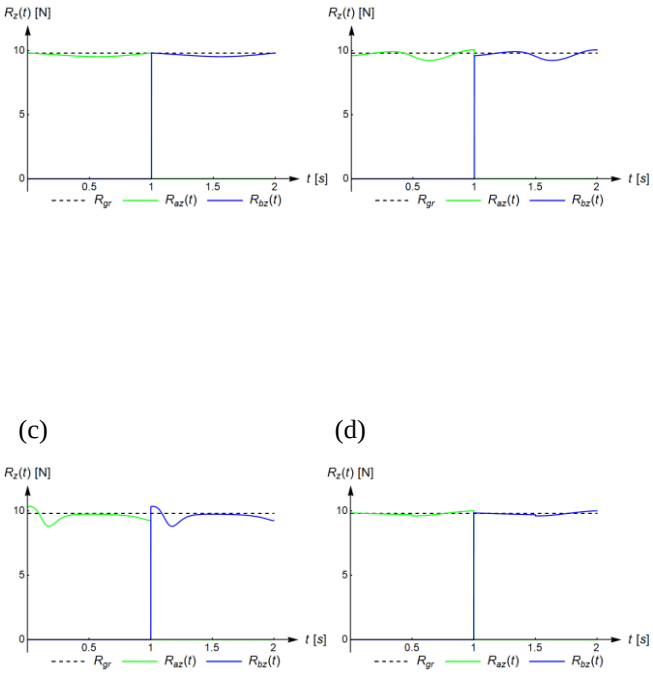

Fig. 21 The components $R_z(t)$ of the ground reaction force acting of the legs of the robot driven by different CPGs: (a) CPG1; (b) CPG2; (c) CPG3; (d) CPG4.

Figure 22 shows curves of the functions $\mu_x(t)$ and $\mu_y(t)$, which are suitable to estimate the minimum value of the friction coefficient between the ground and the feet of the robot, which guarantees that the robot will not slip on the ground during the locomotion process. The smallest oscillations of the values of $\mu_x(t)$ and $\mu_y(t)$ were observed for the proposed CPG4. Therefore, the robot controlled by the proposed model of CPG is able to move on a surface with a relatively low coefficient of friction between its

feet and the ground and without unnecessary accelerations or decelerations in any direction.

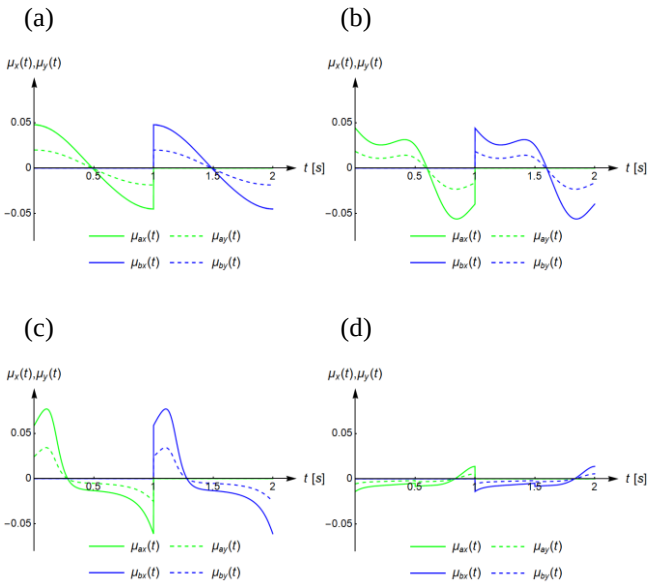

Fig. 22 Time histories of the functions $\mu(t)$ obtained for different CPGs: (a) CPG1; (b) CPG2; (c) CPG3; (d) CPG4.

In further analysis we computed abovementioned the minimum value of the friction coefficient $\mu_{\min}$ between the ground and the feet of the robot, which guarantees that the robot will not slip on the ground during locomotion process, in the following way

$$\mu_{\min} = \max_{t\in[0,T]} \mu_a(t) = \max_{t\in[0,T]} \mu_b(t)\,, \tag{43}$$

since, the functions $\mu_a(t)$ and $\mu_b(t)$ are similar in the rhythmic phase of gait, i.e., they are only shifted in time. Moreover, taking into account the adopted assumptions introduced in Section 2, the coefficient $\mu_{\min}$ is the same for all robot's legs. Time histories of $\mu_a(t)$ and $\mu_b(t)$, and values of the parameter $\mu_{\min}$ for all tested CPGs are presented in Fig. 23.

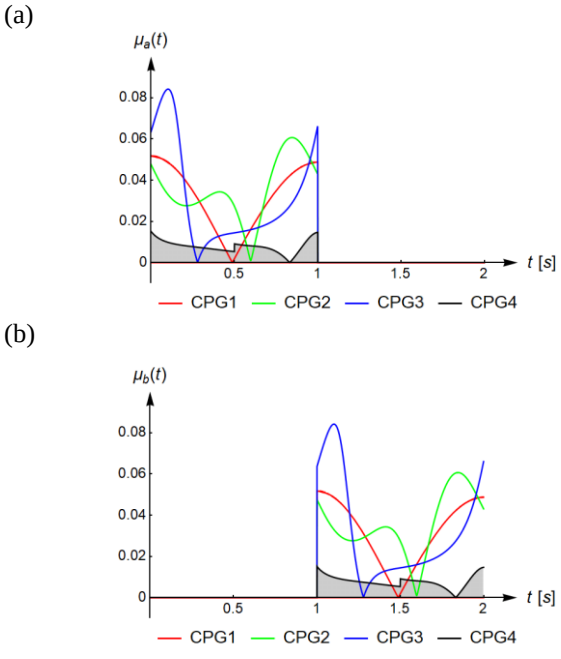

(c)

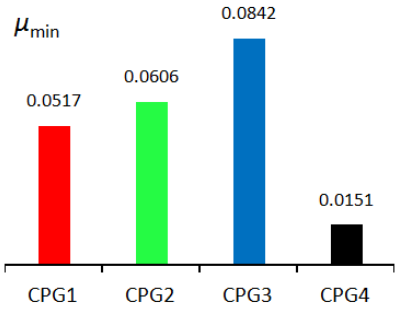

Fig. 23 Time histories of the function $\mu_a(t)$ (a) and $\mu_b(t)$ (b) in different phases of a single robot stride, and the coefficient $\mu_{\min}$ (c) calculated for different CPGs.

In our study, we also considered the problem of planning the trajectory of the robot (i.e., the coordinates $x_C(t)$, $y_C(t)$, $z_C(t)$ in the global coordinate system $Oxyz$) during the walking process of the robot. Here we studied only the robot driven by the proposed model of CPG, i.e., CPG4. In our model, the forward and lateral fluctuations of the robot are controlled by the value of the angle θ, whereas the vertical fluctuations of the robot are controlled by regulating the function $h(t)$. The possibility of controlling the direction of the robot movement by changing the value of the angle θ has been already presented in detail in Section 4. This is why, in this section, we focused only on the ability to control the robot movement in the vertical direction. Therefore, as an example, we used $\theta = \pi/8$ and $h(t) = (0.21 - 0.1e^{-0.3t}\sin 2t + 0.015t)$ m. Moreover, we also considered initial and terminal phases of the robot gait, i.e., the change in the configuration of the robot's legs during the transition from the initial configuration (the same configurations of all legs) to the rhythmic phase of gait (n full cycles), as well as the transition from the rhythmic phase of gait to the initial phase of gait, respectively. To do it, both the length and the height of a single robot stride in were calculated from the following formula

$$l_{\text{stride}}(t) = l_{\max} P(t)\,, \tag{44}$$

$$h_{\text{stride}}(t) = h_{\max} P(t)\,, \tag{45}$$

where $l_{\max}$ and $h_{\max}$ denote the maximum length and height of a single robot stride, respectively, whereas $P(t)$ is a function given by the following relation

$$P(t) = \begin{cases} \dfrac{2}{T}t & \text{if} \quad t\in[0,\, 0.5T], \\ 1 & \text{if} \quad t\in(0.5T,\, (n{+}0.5)T], \\ 1-\dfrac{2}{T}(t-(n{+}0.5)T) & \text{if} \quad t\in((n{+}0.5)T,\, (n{+}1)T]. \end{cases} \tag{46}$$

As a result, we considered the proposed CPG model in the following form

$$\begin{cases} u_a(t) = f_x\left(t_m(t)\right), \\ v_a(t) = f_{za}\left(t_m(t)\right), \\ u_b(t) = -u_1(t), \\ v_b(t) = f_{zb}\left(t_m(t)\right), \end{cases} \tag{47}$$

where

$$t_m(t) = \begin{cases} 0.5\,\mathrm{mod}(t,T) & \text{if} \quad t \in [0,\ 0.5T] \cup ((n+0.5)T,\ (n+1)T], \\ \mathrm{mod}(t-0.25T,T) & \text{if} \quad t \in (0.5T,\ (n+0.5)T]. \end{cases} \tag{48}$$

The simulated configurations of the robot walking on a planar surface, moving in the vertical direction due to the function $h(t)$, captured at regular time intervals, are illustrated in Fig. 24. As can be seen, the supporting legs touch the ground, while the vertical position of the point C of the robot is accurately reflected based on the defined function $h(t)$. As a result, we can control the position of the center of the robot's trunk (marked by point C) in all directions, which can be useful to control walking of the robot in the natural environment.

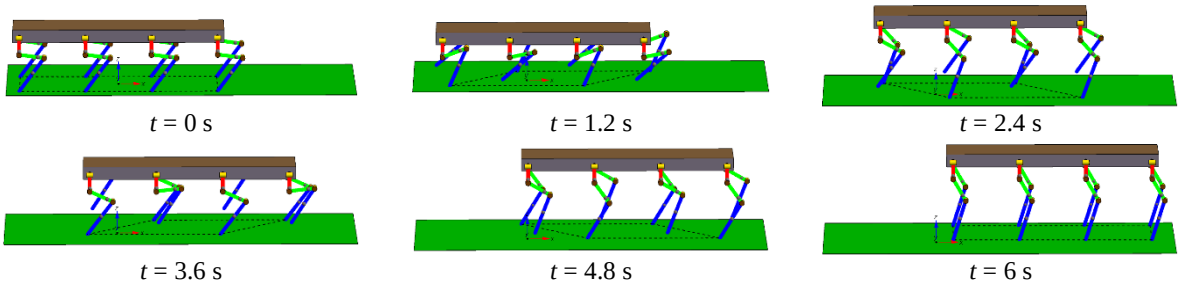

Fig. 24 Simulated configurations of the investigated robot in different phases of gait during walking according to the planned trajectory in the forward, lateral and vertical directions, captured at regular time intervals.

Figures 25-26 present some kinematic and dynamic dependencies of the parameters of the walking robot, which indicate the influence of forward, lateral and vertical fluctuations of the robot on its kinematic and dynamic parameters. Figure 25 shows time histories of articulated angles applied to the joints of the robot's legs. As can be seen, the presented time histories have irregular character resulting from the time-varying function $h(t)$. Figure 26 shows fluctuations in displacements $x_C(t)$, $y_C(t)$, $z_C(t)$ and velocities $v_{xC}(t)$, $v_{yC}(t)$, $v_{zC}(t)$ of the walking robot. The presented time histories can be divided into three phases of gait, namely: the initial phase of gait (t = 0...1 s), the rhythmic gait with two cycles (t = 1...5 s) as well as the terminal phase of gait (t = 5...6 s). In the first, initial phase of gait, speeds of the robot in the forward and lateral direction increase linearly, i.e., from 0 to $2l_{\mathrm{stride}}\cos\theta/T$ = 0.092 m/s and $2l_{\mathrm{stride}}\sin\theta/T$ = 0.038 m/s, respectively. It the second, rhythmic phase of gait, these speeds are constant (0.092 m/s and 0.038 m/s, respectively). In turn, in the last, terminal phase, these speeds decrease linearly from 0.092 m/s to 0 and from 0.038 m/s to 0, respectively. As a result, fluctuations in the robot speeds are not observed, which has a significant and positive impact on the robot stability and its other dynamical parameters. When it comes to vertical fluctuation $z_C(t)$ in the robot position, it is accurately reflected based on the function $h(t)$.

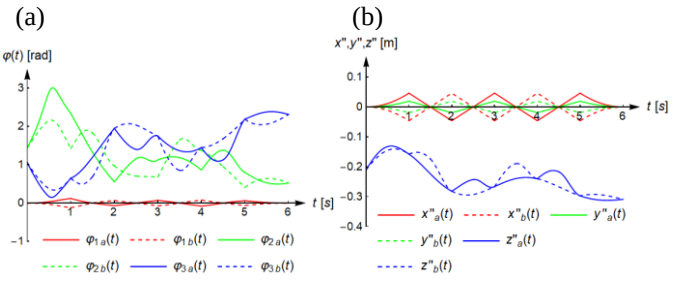

Fig. 25 Time histories of angular positions applied to individual joints of the legs (a) and positions of the robot's feet, plotted in the local coordinate system O"x"y"z" of a single robot's leg.

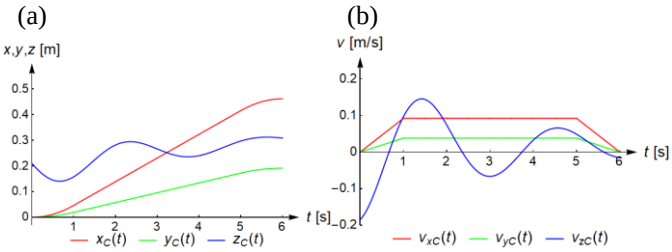

Fig. 26 Time histories of the displacements $x_C(t)$, $y_C(t)$, $z_C(t)$ of the robot's center C (a) and velocities $v_{xC}(t)$, $v_{yC}(t)$, $v_{zC}(t)$ of the robot's center C (b) in the forward, lateral and vertical directions, respectively.

6. Conclusions

In this paper, we have investigated numerically a bio-inspired model of a mammal-like octopod, including kinematic/dynamic parameters of the robot locomotion, its stability, and the possibility of controlling during walking. The simulation model of the robot has been developed in Mathematica and the gait has been generated by four different models of CPG. The proposed CPG model is relatively simple in comparison to the other three investigated CPGs constructed based on the nonlinear oscillators. For instance, our CPG model does not require solving nonlinear differential equations, and it is especially advantageous during the implementation of the CPG in the form of a program written for a microcontroller with limited computing power. Moreover, the proposed model does not produce unnecessary fluctuations in the velocity both in the vertical and horizontal (i.e., movement and lateral) directions of the robot. As a result, it has also a positive impact on the dynamical parameters of the robot. In the case of practical realization of the control system of the robot, some deviations can be present, which can be caused by control errors, dynamics of drives installed in the individual robot's joints, etc. In our future investigations, for instance, more

detailed cases of the robot gait and control of the position of the robot walking on irregular terrains are worth taking into account. Although in our study we adopted some assumptions to simplify the dynamic model of the robot, the obtained results are sufficient to compare the crucial dynamic parameters of the studied octopod robot. Eventually, the proposed method can be simply adapted to control other walking machines such as bipeds, quadrupeds or hexapods.

Acknowledgements

The work has been partially supported by the National Science Centre of Poland under the grant OPUS 9 no. 2015/17/B/ST8/01700 for years 2016-2018.

References

[1] F. Tedeschi, G. Carbone, Design of a novel leg-wheel hexapod walking robot, *Robotics*, Vol. 6, No. 4, pp. 40, 2017.

[2] K. Lagaza, A. Pandey, A literature review on motion planning of hexapod machines using different soft computing methods, *Global Journal of Engineering, Science and Social Science Studies*, Vol. 3, No. 1, pp. 1-10, 2018.

[3] X. Chen, L. Wang, X. Ye, G. Wang, H. Wang, Prototype development and gait planning of biologically inspired multi-legged crablike robot, *Mechatronics*, Vol. 23, No. 4, pp. 429-444, 2013.

[4] G. Chen, B. Jin, Y. Chen, Tripod gait-based turning gait of a six-legged walking robot, *Journal of Mechanical Science and Technology*, Vol. 31, No. 3, pp. 1401-1411, 2017.

[5] D. Grzelczyk, J. Awrejcewicz, Modeling and control of an eight-legged walking robot driven by different gait generators, *International Journal of Structural Stability and Dynamics*, Vol. 19, No. 5, pp. 1941009-1 - 1941009-23, 2019.

[6] D. Grzelczyk, O. Szymanowska, J. Awrejcewicz, Kinematic and dynamic simulation of an octopod robot controlled by different central pattern generators, *Proceedings of the Institution of Mechanical Engineers, Part I: Journal of Systems and Control Engineering*, Vol. 233, No. 4, pp. 400-417, 2019.

[7] A. Mahapatra, S.S. Roy, Computer aided dynamic simulation of six-legged robot, *International Journal of Recent Trends in Engineering*, Vol. 2, No. 2, pp. 146-151, 2009.

[8] X. Rong, Y. Li, J. Ruan, B. Li, Design and simulation for a hydraulic actuated quadruped robot, *Journal of Mechanical Science Technology*, Vol. 26, No. 4, pp. 1171-1177, 2012.

[9] W. Chen, G. Ren, J. Zhang, J. Wang, Smooth transition between different gaits of a hexapod robot via a central pattern generators algorithm, *Journal of Intelligent & Robotic Systems*, Vol 67, No. 3-4, pp. 255-270, 2012.

[10] Ig Mo Koo, Tran Duc Trong, Tae Hun Kang, GiaLoc Vo, Young Kuk Song, Chang Min Lee, Hyouk Ryeol Choi, 2007, Control of a quadruped walking robot based on biologically inspired approach, in: *Proceedings of the 2007 IEEE/RSJ International Conference on Intelligent Robots and Systems*, San Diego, CA, USA, October 29 – November 2, 2007, 2969-2974.

[11] Ig Mo Koo, Tae Hun Kang, Gia Loc Vo, Tran Duc Trong, Young Kuk Song, Hyouk Ryeol Choi, Biologically inspired control of quadruped walking robot, *International Journal of Control, Automation and Systems*, Vol. 7, No. 4, pp. 577-584, 2009.

[12] S.S. Roy, D.K. Pratihar, Kinematics, dynamics and power consumption analyses for turning motion of a six legged robot, *Journal of Intelligent & Robotic Systems*, Vol. 74. No. 3-4, pp. 663-688, 2014.

[13] V.A. Makarov, E.D. Rio, M.G. Bedia, M.G. Velarde, W. Ebeling, Central pattern generator incorporating the actuator dynamics for a hexapod robot, *International Journal of Electrical and Computer Engineering*, Vol. 2. No. 3, pp. 498-503, 2008.

[14] M. Vukobratovic, B. Borovac, Zero-Moment point – thirty five years of its live, *International Journal of Humanoid Robotics*, Vol. 1, No. 1, pp. 157-173, 2004.

[15] J.H. Park, Y.K. Rhee, ZMP trajectory generation for reduced trunk motions of biped robots, in: *Proceedings of IEEE/RSJ International Conference on Intelligent Robots and Systems (IROS'98)*, Victoria, Canada, 1998, 90-95.

[16] A.D. Kuo, The relative roles of feedforward and feedback in the control of rhythmic movements, *Motor Control*, Vol. 6, No. 2, pp. 129-145, 2002.

[17] K. Nakada, T. Asai, Y. Amemiya, An analog neural oscillator circuit for locomotion controller in quadruped walking robot, in: *Proceedings of the International Joint Conference on Neural Networks*, Portland, OR, USA, 20-24 July 2003, 2: 983-988 (10.1109/IJCNN.2003.1223824), 2003.

[18] S.L. Hooper, Central pattern generators, *Current Biology*, Vol. 10, No. 5, pp. R176-R179, 2000.

[19] S. Rossignol, Locomotion and its recovery after spinal injury, *Current Opinion in Neurobiology*, Vol. 10, No. 6, pp. 708-716, 2000.

[20] J. Buchli, L. Righetti, A.J. Ijspeert, Engineering entrainment and adaptation in limit cycle systems - from biological inspiration to applications in robotics, *Biological Cybernetics*, Vol. 95, No. 6, pp. 645-664, 2006.

[21] A.C. de Pina Filho, M.S. Dutra, Application of hybrid van der Pol-Rayleigh oscillators for modeling of a bipedal robot, in: *Mechanics of Solids in Brazil 2009*, edited by H.S. da Costa Mattos, Marcílio Alves, Brazilian Society of Mechanical Sciences and Engineering, ISBN 978-85-85769-43-7, 209-221, 2009.

[22] V.A. Makarov, W. Ebeling, M.G. Velarde, Soliton-like waves on dissipative toda lattice, *International Journal of Bifurcation and Chaos*, Vol. 10, No. 5, pp. 1075-1089, 2000.

[23] A. Dvorak, P. Kuzma, P. Perlikowski, V. Astakhov, T. Kapitaniak, Dynamics of three Toda oscillators with nonlinear unidirectional coupling, *The European Physical Journal Special Topics*, Vol. 222, No. 10, pp. 2429-2439, 2013.

[24] A. Dvorak, V. Astakhov, P. Perlikowski, T. Kapitaniak, Nonlinear resonance and synchronization in the ring of unidirectionally coupled Toda oscillators, *The European Physical Journal Special Topics*, Vol. 225, No. 13-14, pp. 2635-2643, 2016.

[25] S. Rutishauser, L. Righetti, A.J. Ijspeert, Passive compliant quadruped robot using central pattern

generators for locomotion control, in: *Proceeding of the 2nd Biennial IEEE/RAS-EMBS International Conference on Biomedical Robotics and Biomechatronics*, 19-22 October 2008, Scottsdale, AZ, USA, 710-715, 2008.

[26] K. Seo, S-J. Chung, J-J.E. Slotine, CPG-based control of a turtle-like underwater vehicle, *Autonomous Robots*, Vol. 28, No. 3, pp. 247-269, 2010.

[27] B. Zhong, S. Zhang, M. Xu, Y. Zhou, T. Fang, W. Li, On a CPG-based hexapod robot: amphiHex-II with variable stiffness legs, *IEEE/ASME Transactions on Mechatronics*, Vol. 23, No. 2, pp. 542-551, 2018.

[28] Y. Zhu, Y. Wu, Q. Liu, T. Guo, R. Qin, J. Hui, A backward control based on σ-Hopf oscillator with decoupled parameters for smooth locomotion of bio-inspired legged robot, *Robotics and Autonomous Systems*, Vol. 106, pp. 165-178, 2018.

[29] P. Veskos, Y. Demiris, Robot swinging using van der Pol nonlinear oscillators, in: *Proceedings of the Third International Symposium on Adaptive Motion of Animals and Machines*, September 25-30, 2005, Ilmenau, Germany, 4 pages, 2005.

[30] P. Veskos, Y. Demiris, Experimental comparison of the van der Pol and Rayleigh nonlinear oscillators for a robotic swinging task, in: *Proceedings of the AISB 2006 Conference, Adaptation in Artificial and Biological Systems*, 3-6 April 2006, Bristol, England, 197-202, 2006.

[31] C. Liu, Q. Chen, J. Zhang, Coupled van der Pol oscillators utilised as central pattern generators for quadruped locomotion, in: *Proceedings of the 2009 Chinese Control and Decision Conference*, 17-19 June 2009, Guilin, China, 3677-3682, 2009.

[32] N. Kuwata, Y. Hoshi, B.T. Nohara, Analysis of coupled van der Pol oscillators and implementation to a myriapod robot, in: *Proceedings of the 17th World Congress The International Federation of Automatic Control*, Seoul, Korea, July 6-11, 2008, 767-772..

[33] M. Piątek, A. Turnau, Hexapod - six-legged walking robot controlled with Toda-Rayleigh lattice, *Bio-Algorithms and Med-Systems*, Vol. 8, No. 1, pp. 111-121, 2012.

[34] J. Nishii, Legged insects select the optimal locomotor pattern based on the energetic cost, *Biological Cybernetics*, Vol. 83, No. 5, pp. 435-442, 2000.